

# Using on Results of External Heat Exchange Local Coefficients Study for Formation of Hydrodynamic Structure of Fluidized Bed Optimal for Burning Low Grades Solids Fuels

RAFAIL ISEMIN, DMITRY KLIMOV, SERGEY KUZMIN, ALEKSANDR MIKHALEV,  
VALENTIN KONYAKHIN, OLEG MILOVANOV, NATALIA MURATOVA

Bio center

Tambov State Technical University

Sovetskaya street, 106, Tambov, 392000

RUSSIA

penergy@list.ru

<http://www.uicb.ru>

*Abstract:* - The type of air entry distribution is essential in the formation of hydrodynamic structures of fluidized bed. The present study is aimed to form a hydrodynamic structure of fluidized bed optimal for burning low-grade solids fuels. In order to determine the uniformity of the fluidized bed in the bed heat exchange rate between the bed and a heat exchange member immersed therein was measured. At a first approximation, heat exchange with the member immersed into the bed imitates heat exchange between the fluidized bed and a fuel particle. It is allowed to determine that an optimal hydrodynamic structure of the bed can be formed by using a lattice supplying the major portion of air near the furnace wall. The above conclusion was confirmed by experiments using a real furnace with a fluidized bed.

*Key-Words:* - Air distribution, anthracite culm, biomass, combustion, fluidized bed, heat transfer, straw pellets

## 1 Introduction

The use of fluidization technique in heat-and-power engineering provides a comprehensive solution for reducing environmental pollution with noxious emissions, reducing size and metal consumption of boiler units, and increasing reliability thereof without excessive fuel quality and performance stability requirements [1, 2].

## 2 Problem Formulation

However, the hydrodynamic structure of fluidized bed is far from uniform, and said non-uniformity increases further along with an increase in the amount of fluidization. In industrial scale apparatuses, fluidization gas can be supplied via regularly spaced but discrete devices (nozzles, tubes, etc.). In this case, gas bubbles would rise along certain preferred lines, and local vertical solid particle circulation cells would form, hindering complete mixing of particles and gas in the bed [3, 4, 5, 6]. With regards to combustion of fine solids fuels and solid fuels with high volatile matter content, the formation of preferred gas bubble

ascent lines can lead to burning of fine solids particles and gas flare formation that penetrates the bed and burns chaotically in the freeboard [3].

## 3 Problem Solution

Particle movement in a fluidized bed can be affected by providing non-uniform entry gas distribution through a distribution lattice. The above method provides strong circulatory particle movement of "Gulfstream movement" type and more effective gas mixing in the bed when supplying greater gas flow through the peripheral area of the gas distribution lattice, as opposed to the central area thereof [3].

Evidently, the approach of providing intensive internal particle circulation in the bed by means of irregular air entry distribution is the simplest and most effective solution. However, results of systematic studies of hydrodynamic structure of fluidized bed with the purpose of discovering optimal air entry distribution in the context of liquid fuel combustion and combustion of fuels with high volatile matter content are not yet available.

The object of the present study is to carry out such studies.

### 3.1 Methods and equipment

The hydrodynamic structure of a fluidized bed can be studied using various methods, each having certain advantages and disadvantages [7, 8, 9, 10, 11, 12, 13, 14, 15, 16, 17, 18].

The results of a fluidized bed hydrodynamic structure study based on measuring heat exchange rate between the bed and a heat exchange member immersed therein (in various areas of the fluidized bed) are of particular practical interest. At a first approximation, heat exchange with the member immersed into the bed imitates heat exchange between the fluidized bed and a fuel particle, which is important for evaluation of heating and combustion velocity of the fuel particle in the bed, as well as for eliminating local overheating of the bed, fuel ash fusion and bed defluidization.

External heat exchanged between the fluidized bed and the surface (copper ball  $D = 24$  mm) was measured using a conventional regular temperature conditions method [19]. A type L thermocouple was welded into the ball center, said thermocouple allowing for continuous temperature measurement of the pre-heated ball after immersing it into the cold fluidized bed. The sensor is shown schematically in Fig. 1.

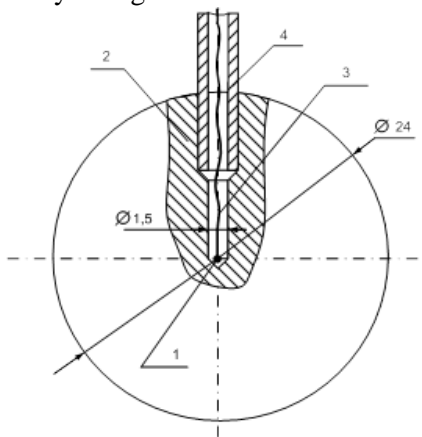


Fig. 1. Diagram of sensor for determining heat exchange rate

- 1 – thermocouple head with diameter of 1.2 mm,
- 2 – copper ball, 3 – thermocouple cables,
- 4 – connecting tube with diameter of 3.0 mm

In order to determine heat exchange coefficient distribution in the fluidized bed, a sensor positioning system shown in Fig. 2 was used. The sensor positioning system in the fluidized bed chamber allows placing the copper ball both on chamber axis and at a variable distance  $x$  from the axis. The height  $h$  of the ball position above the gas distribution lattice was adjustable. During the experiments, the sensor was placed at a height of 30 mm and 80 mm above the lattice. Quartz sand with

particle size of 0.5...0.8 mm was used as the particulate material ( $d = 0.65$  mm;  $u_{mf} = 0.26$  m/s).

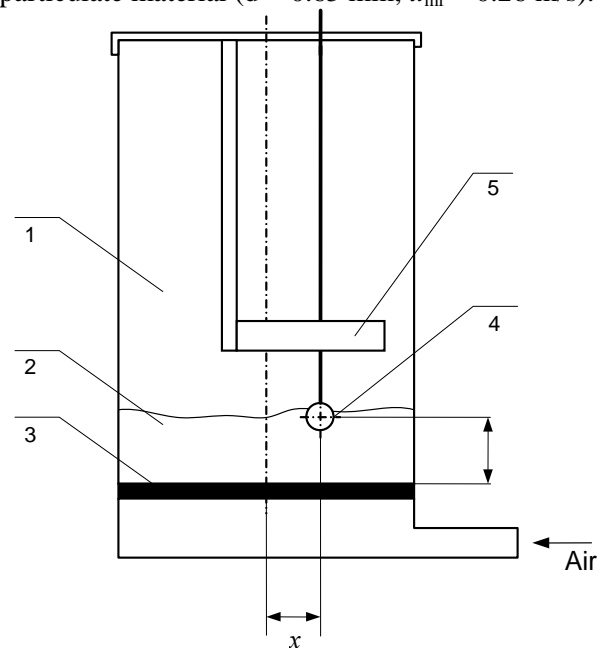


Fig. 2: Diagram of sensor arrangement for measuring heat exchange rate in a fluidized bed.  
1 – chamber with fluidized bed, 2 – fluidized bed of sand, 3 – gas distribution lattice, 4 – sensor, 5 – sensor positioning system

In order to provide various types of air entry distribution, three perforated lattices were used. The first configuration of lattice comprises a regular open area (the lattice forms a "flat" air velocity profile at bed entry), the second configuration comprises a greater open area in the center of lattice (the lattice forms a "convex" entry air velocity profile), and in the third configuration, the greater open area is arranged at the periphery (the lattice forms a "concave" entry air velocity profile). The lattice is shown schematically in Fig 3, and characteristics thereof are provided in Table 1.

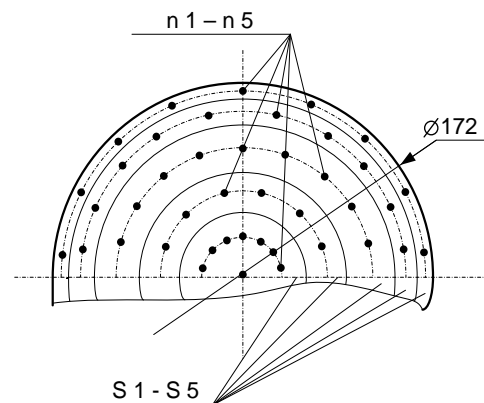


Figure 3: Gas distribution lattice diagram  
n1- n5 – number of openings in zones, S1 - S5 – zones of identical surface area

center of the apparatus and at half-radius point

Table 1: Distribution of openings in various lattices

Lattice zones with identical surface area	Configuration 1		Configuration 2		Configuration 3	
	Open area ratio, %	Number of openings with diameter of 2 mm, n	Open area ratio, %	Number of openings with diameter of 2 mm, n	Open area ratio, %	Number of openings with diameter of 2 mm, n
S1 3919 mm <sup>2</sup>	1.5	19	2.5	32	0.5	7
S2 3919 mm <sup>2</sup>	1.5	19	2.0	25	1.0	13
S3 3919 mm <sup>2</sup>	1.5	19	1.5	19	1.5	19
S4 3919 mm <sup>2</sup>	1.5	19	1.0	13	2.0	25
S5 3919 mm <sup>2</sup>	1.5	19	0.5	7	2.5	32

Prior to measurement, the copper ball was heated with a hot air source to 200-240°C, then the ball was immersed into target location in the bed, and the reduction in copper ball temperature was determined until the temperature equaled that of the fluidized bed. In order to determine the effect of air velocity in the chamber, all experiments were carried out at three different air filtering velocities  $u = 0.49$ ; 0.61 and 0.73 m/s.

### 3.2 Results and discussion

Figures 4.1 - 4.3 show mean values of heat exchange coefficients between the sensor and the fluidized bed for three types of air distribution lattice and two initial bed height values (0.05 m and 0.1 m).

In case of the "flat" entry air velocity profile (Fig. 4.1), the hydrodynamic structure of the bed was non-uniform due to the fact that at the initial bed height of 0.05 m and air velocity of 0.49 m/s, heat exchange rate near the wall of the apparatus is 1.31 times higher than that in the center of the apparatus. An increase in air velocity to 0.61 m/s does not lead to an increase in uniformity, as the heat exchange coefficient value at half-radius point of the apparatus is 1.19 times lower than near the apparatus wall. Finally, at air velocity of 0.73 m/s, the non-uniformity is maintained, as the heat exchange rate in the center of the apparatus is 1.16 times higher than in other zones of the fluidized bed.

In case of the "flat" entry air velocity profile, the non-uniformity of the fluidized bed hydrodynamic structure is maintained when the initial bed height is increased to 0.1 m, as the heat exchange rate in the

thereof is 1.1 - 1.35 times higher than in peripheral zones of the bed. Furthermore, at the initial bed height of 0.1 m, heat exchange rate between the bed and the heat exchange member immersed therein decreases with an increase in the velocity of air being passed through the bed (Fig. 4.1).

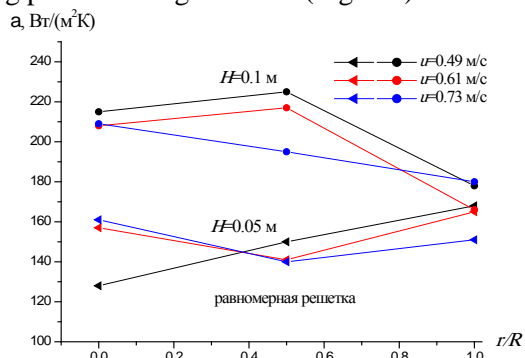


Figure 4.1: Heat exchange coefficient values between the fluidized bed and the heat exchange member plotted against air velocity at uniform entry air distribution (Flat entry air velocity profile).

In case of a "convex" entry air velocity profile, the rate of heat exchange processes in the bed is significantly higher compared to the "flat" entry air velocity profile (Fig. 4.2). At air velocity of 0.49 m/s, the heat exchange rate in the fluidized bed with initial height of 0.05 m is 1.5 - 1.6 times higher than in the "flat" profile at the same air velocity. However, at the initial bed height of 0.05 m, the hydrodynamic structure of the bed remains non-uniform, as at the half-radius point of the apparatus, the heat exchange rate is 1.3 - 1.4 times higher than at the center and near the apparatus wall, respectively. An increase in air velocity to 0.61 m/s leads to an increase in uniformity of the fluidized

bed hydrodynamic structure: heat exchange rate values in this case are in the range of 230 to 280 W/m<sup>2</sup> degr. Said increase can be explained by the fact that a strong circulatory movement forms in the bed, spreading over the entire bed volume. However, a further increase in air velocity to 0.73 m/s leads to a decrease in heat exchange rate to 250 - 270 W/m<sup>2</sup> degr. When the initial bed height is increased to 0.1 m in the "convex" entry air velocity profile, said increase does not in fact affect heat exchange rate and particle movement rate. In other words, the "convex" profile forms a uniform structure with approximately equal particle movement rates over the entire bed volume. However, this is only true for relatively low velocities of air being passed through the bed. When air velocity is increased to 0.73 m/s, a sharp spike in heat exchange rate (up to 400 W/m<sup>2</sup> degr) occurs approximately at the central radial point of the apparatus, whereas heat exchange rate in other zones of the bed remains the same.

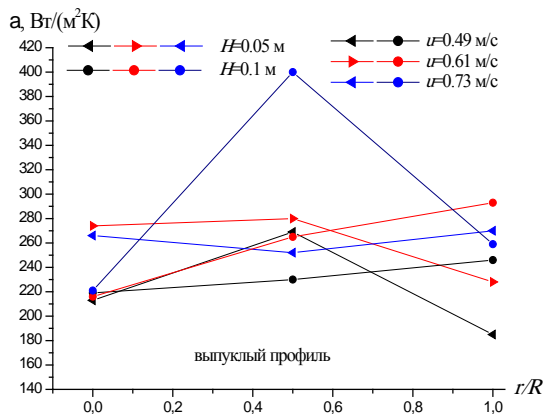


Figure 4.2: Heat exchange coefficient values between the fluidized bed and the heat exchange member plotted against air velocity in a "convex" entry air velocity profile.

In case of a "concave" entry air velocity profile, when air velocity increases, the heat exchange rate also increases when compared to the "flat" entry air velocity profile (Fig. 4.3). However, the case of a "concave" entry air velocity profile, there is a significant non-uniformity in the hydrodynamic structure of the bed with initial height of 0.05 m, which is completely eliminated upon increasing air velocity to 0.73 m/s. When the initial bed height is increased to 0.1 m, the "concave" entry air velocity profile exhibits heat exchange coefficient values fluctuations in an extremely narrow range of 230 to 260 W/m<sup>2</sup> degr, which indicates uniformity of the bed hydrodynamic structure at any velocity of air being passed through the fluidized bed in the studied air velocity range. Furthermore, when using the "concave" entry air velocity profile, at bed height of

0.1 m, the heat exchange rate is 1.5 - 3.5 higher than that in the bed with initial height of 0.05 m.

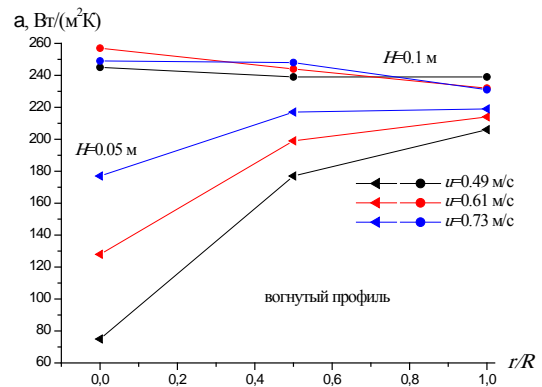


Figure 4.3: Heat exchange coefficient values between the fluidized bed and the heat exchange member plotted against air velocity in a "concave" entry air velocity profile.

It should also be noted that the possibility of maintaining a uniform hydrodynamic structure of the fluidized bed upon an increase in air velocity in the "concave" entry profile suggests that said air velocity profile allows providing a furnace with a wider power adjustment range without decreasing solid fuel combustion efficiency.

### 3.3 Experimental verification of results in practice

In order to verify and substantiate the choice of air distribution lattice forming at the bed entry a "concave" air velocity profile, a prototype furnace was constructed with a fluidized bed with a capacity of 400 kW, the design of which is illustrated in the scheme of Fig. 5.

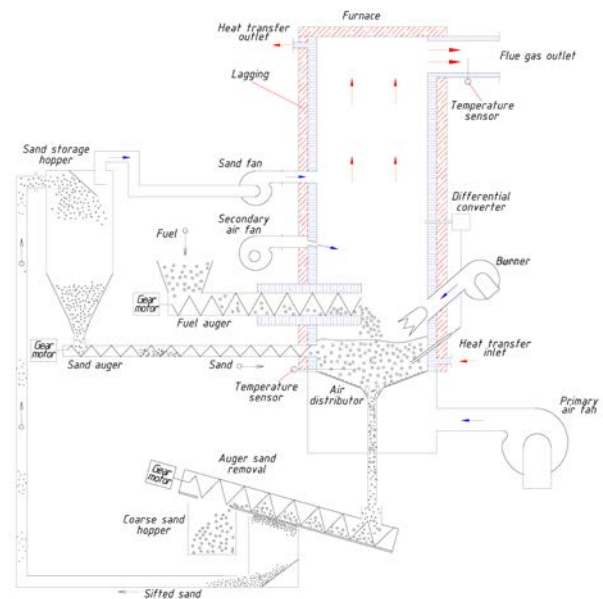


Figure 5. Functional scheme

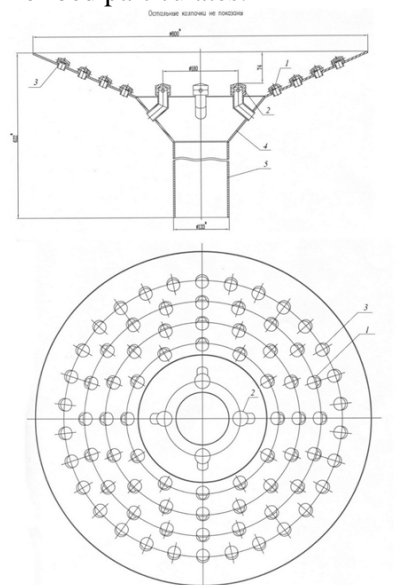
Figure 5 shows an outline of the experimental unit for studying the combustion of different types of solid fuel. The studies are conducted in the remote cylindrical furnace with inner diameter of 800 mm and height of 1500 mm above the air distribution grill. The furnace is water-cooled, and the cooling circuit of the furnace is inserted in the cooling circuit of the heat exchanger of flue gases.

The design of the furnace provides the tangential inlet of flue gases into the combustion can of the exchanger. This provides the post-combustion of volatile matters and the fallout of fuel and ash particles from gas flow.

The furnace is equipped with a hopper for solid fuel and with the device for fuel feeding in the furnace. Fuel inlet in the furnace is carried out at height of 350 mm above the air distribution grill.

The furnace is rested upon the air distribution grill; blasting primary air from the high-pressure fan is forced under this grill.

The diagram illustrating the air distribution lattice of a prototype furnace (Fig. 6) shows the arrangement of caps for supplying blast air. The caps are uniformly arranged over the entire lattice area. However, due to the fact that the air distribution lattice is tilted at 30° towards the center, the resistance of inert material layer or particulate catalyst over the caps arranged on the lattice periphery is lower than that over the central part of the lattice. Therefore, the peripheral part of the lattice experiences greater air flow compared to the central part thereof, thus forming a "concave" entry air velocity profile and providing intensive circulation of bed particulates.



1 – working area caps, 2 – ash discharge area caps, 3 – wall-adjacent caps, 4 – tapered (tilted) lattice floor, 5 – ash discharge manifold.

Figure 6. Air distribution lattice diagram

Caps have different structures. Caps with air outlet openings (5 mm in diameter) are arranged near the ash discharge area. The remaining caps have air inlet openings of 2.5 mm in diameter. Caps arranged in the wall-adjacent area near the furnace unit wall are undercut to facilitate assembly. The remaining caps are working area caps.

The furnace was used to burn straw pellets and anthracite culm with a composition provided in Table 2.

Table 2: The anthracite culm and straw pellets characteristics

Parameter	Anthracite culm	Straw pellets
Diameter, mm	19,76	7.0
Average length, mm	27,9	12.03
Diameter / average length ratio	4,1	0.59
Density, kg/m <sup>3</sup>	4,6	1190
Bulk density, kg/m <sup>3</sup>	0,54	487.9
Combustion value, MJ/kg	2010	15.42
Ash content, %	1280	4.38
Humidity, %	57,8	8.12
Initial ash content, %	1,2	6.87
Higher combustion value, MJ/kg	0,6	16.91
Lower combustion value, MJ/kg	1,3	15.52
Overall chlorine content, % of dry matter	0,1	0.094
Ash deformation temperature, °C	1050	940
Ash softening temperature, °C	1210	980
Ash fusion temperature, °C	1240	1070
Ash melting temperature, °C	1350	1300

The fractional composition of culm: the proportion of particles is larger than 10 mm – 1,45 %; from 3 to 10 mm – 35,61 %; 1 to 3 mm – 26,61 %; from 0.6 to 1 mm, 8,96 %; from 0.2 mm to 0.6 mm is 18: 22C %; less than 0.2 mm is 9.6 %. The ignition temperature of the volatiles released from culm was 690 °C.

The furnace was tested in nominal operation. During testing, a «VarioPlus» gas analyzer was continuously used to measure oxygen and carbon monoxide content in furnace gas at furnace exit.

Figures 7 to 12 show change curves of the temperature of flue gases at the outlet of the furnace; the coefficient of excess air for the combustion device; carbon monoxide, nitric oxide, nitrogen oxides and sulfur oxides during combustion of anthracite culm.

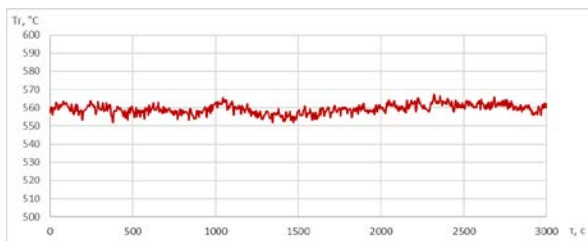


Figure 7. The temperature change of furnace gas at furnace exit during combustion of anthracite culm

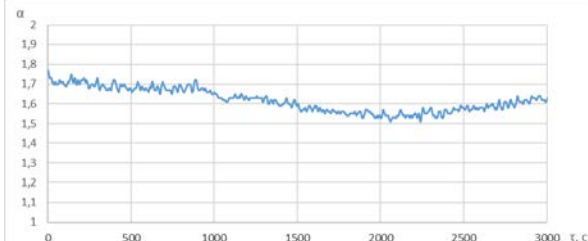


Figure 8. The coefficient of excess air change in furnace gas at furnace exit during combustion of anthracite culm

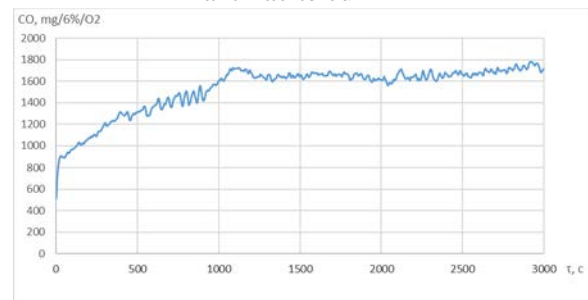


Figure 9. The content of carbon monoxide change in furnace gas at furnace exit during combustion of anthracite culm

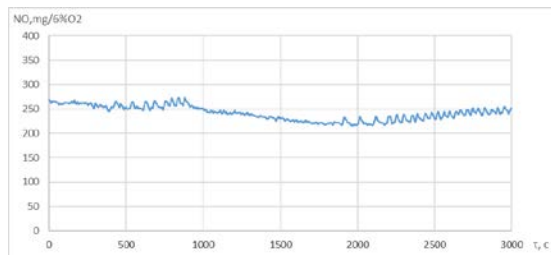


Figure 10. The content of nitrogen monoxide change in furnace gas at furnace exit during combustion of anthracite culm

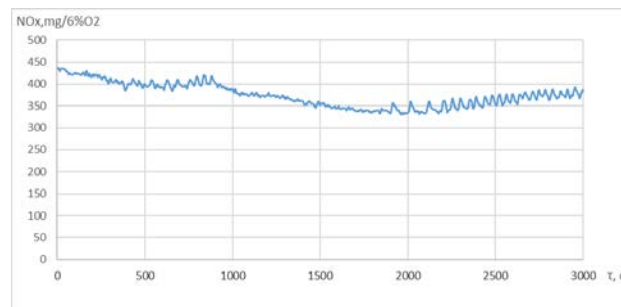


Figure 11. The content of nitrogen oxides change in furnace gas at furnace exit during combustion of anthracite culm

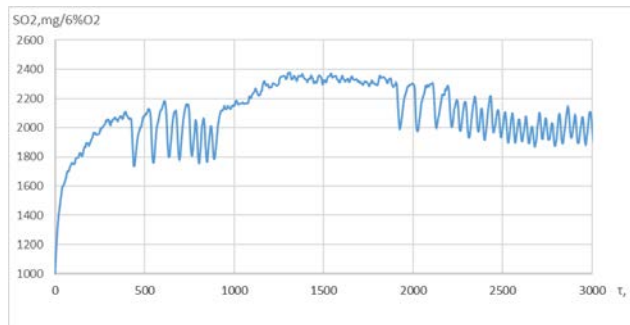


Figure 12. The content of sulfur oxide change in furnace gas at furnace exit during combustion of anthracite culm.

Although the temperature of the gases at the outlet of the furnace (figure 7) did not exceed 570 °C, the combustion of culm was stable.

The low combustion temperature of culm led to the low emissions of nitric oxide (approximately 133 mg/m<sup>3</sup> when the content of oxygen in flue gases equals 11.4 percent) and nitrogen oxides (approximately 197 mg/m<sup>3</sup> when the content of oxygen in the flue gas equals 11.4 %), these results correspond to the findings of other scientists. [20, 21].

On the other hand, the content of the CO (approximately 900 mg/m<sup>3</sup> when the concentration of oxygen equals 11.4 %) was sufficiently high.

The emissions of oxides of sulfur were particularly high (approximately 1052 mg/m<sup>3</sup> when the concentration of oxygen equals 11.4 %). This can be explained by two factors: 1) the high sulfur content in the initial culm (1,25 %), 2) almost complete entrainment of ash from the bed.

The latter circumstance leads to the fact that ash does not accumulate in the bed and its potassium-containing components cannot be used for the binding of sulfur oxides.

Speaking of the emission of sulfur oxides, it should be noted that the similar phenomenon was already observed by other researchers [20] during combustion of anthracite culm.

The burning of the straw pellets was happening at the gas temperature of 605-625°C at furnace exit (Figure 13).

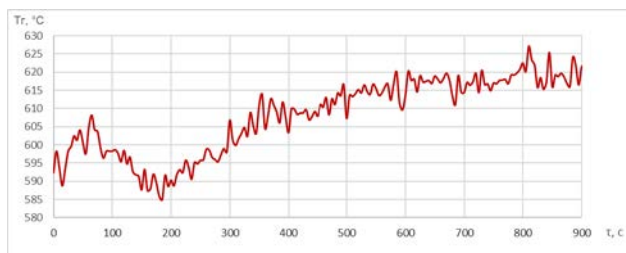


Figure 13. The temperature change of furnace gas at furnace exit during combustion of straw pellets.

The excess air coefficient at furnace exit (Figure 14) is supported at a higher level; the same during combustion of anthracite culm ( $\alpha = 2,1 - 2,2$ ).

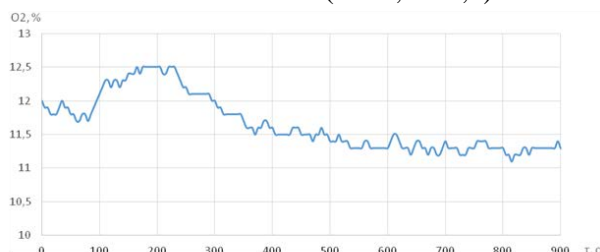


Figure 14. Oxygen content change in furnace gas at furnace exit during combustion of straw pellets.

As can be seen from figure 15, the burning of straw pellets in the experimental furnace with fluidized bed is accompanied by an extremely low emission of CO in the atmosphere (100 – 160 mg/m<sup>3</sup> when the concentration of oxygen in flue gases equals 6 % or 52 – 84 mg/m<sup>3</sup> when the concentration of oxygen in the flue gas equals 11.4 %).

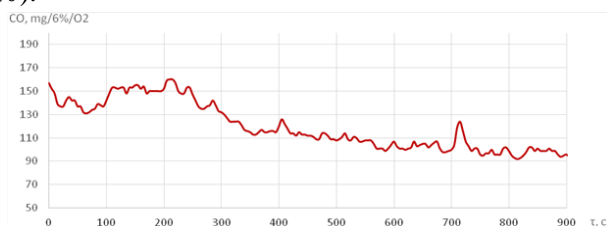


Figure 15. Carbon monoxide content change in furnace gas at furnace exit during combustion of straw pellets.

When burning the straw pellets, the content of nitrogen monoxide ranges from 500 – 600 mg/m<sup>3</sup> (figure 16) or from 260 – 315 mg/m<sup>3</sup> when oxygen concentration equals 11.4%. The average concentration of NO<sub>x</sub> is 750 mg/m<sup>3</sup> (Figure 17) or 394 mg/m<sup>3</sup> when the concentration of oxygen in combustion gases equals 11,4%.

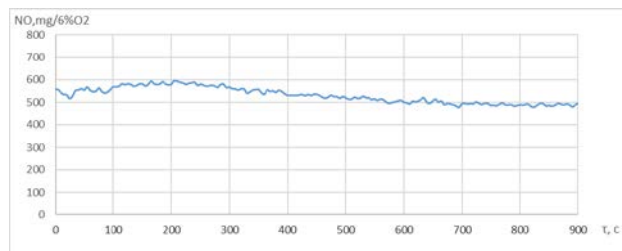


Figure 16. Nitrogen monoxide content change in furnace gas at furnace exit during combustion of straw pellets

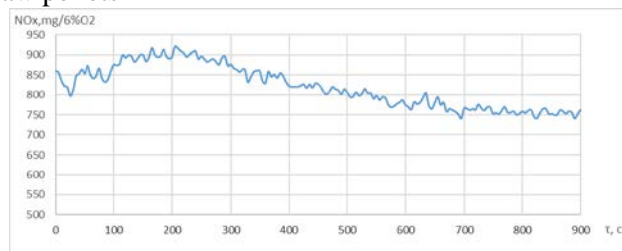


Figure 17. Nitrogen oxides content change in furnace gas at furnace exit during combustion of straw pellets.

The content of sulfur oxides during combustion of straw pellets was almost equal to zero.

## 4 Conclusion

Conducted studies of changes in the values of local heat transfer coefficients in a fluidized bed allowed to choose the type of air entry distribution as the optimum for combustion solid fuel with a high volatile matter content and solid fuels with small particles.

Selected type of air entry distribution supplying the major portion of air near the furnace wall. It provides intensive circulation of solid particles and gas in the bed.

This intense circulation provides almost complete combustion of the volatile matter in the bed volume and low emissions of carbon monoxide in the atmosphere by burning biofuels.

On the other hand, the intense circulation of particles in the bed creates conditions for stable ignition and combustion of anthracite culm, which is low reactivity and high ash fuel.

This work was financially supported by the Ministry of Education and Science of Russia (Agreement № 14.577.21.0116 on October 20, 2014, Unique identifier for Applied Scientific Research (project) RFMEFI57714X0116)

### References:

- [1] Borodulya A.V., Vinogradov L.M., *Combustion of Solid Fuel in Fluidized Bed*, Nauka i Technika, 1980.

- [2] Radovanovic M., *Combustion of Fuel in a Fluidized Bed*, Energoatomizdat, 1990.
- [3] Eights J., *Basics Mechanics of fluidization with applications*, Mir, 1986.
- [4] Uhimann M., Pinelli A., Direct numerical simulation of vertical particulate channel flow in the turbulent regime, *Poceedining on 20th International conference on fluidized bed combustion*, X'ian, China, 2009, pp. 83-96.
- [5] Liu D.Y., Chen X.P., Liang C., Zhao C.S., Solids mixing in the bottom zone of fluidized bed, *Poceedining on 20th International conference on fluidized bed combustion*, X'ian, China, 2009, pp. 459-463.
- [6] Tian C., Wang Q., Lun Z., Zhang X., Cheng L., Ni M., Cen K., Effect of riser geometry structure on local flow pattern in a rectangular circulation fluidized bed, *Poceedining on 20th International conference on fluidized bed combustion*, X'ian, China, 2009, pp. 464-470.
- [7] Deigado S., Briongos J. V., Accosta-Iborra A., Santana D., Multiple Orifice Bubble Generation in Gas-Solid Fluidized Beds: The Activation Region Approach, *Proceeding on International Conference FLUIDIZATION XIII – New Paradigm in Fluidization Engineering*, 2010, pp. 73-80.
- [8] Nawaz Z., Sun Y., Chu Y., Wei F., Mixing Behavior and Hydrodynamic Study of Gas-Solid-Solid Fluidization System: Co-Fluidization on FCC and Coarse Particles, *Proceeding on International Conference FLUIDIZATION XIII – New Paradigm in Fluidization Engineering*, 2010, pp. 97-104.
- [9] Olsson J., Pallares D., Johnsson F., Digital Image Analysis of Bubble Distribution, *Proceeding on International Conference FLUIDIZATION XIII – New Paradigm in Fluidization Engineering*, 2010, pp. 177-184.
- [10] Cocco R., Shaffer F., Karri S.B.R., Hays R., Knowlton T. Particle Clusters in Fluidized Bed, *Proceeding on International Conference FLUIDIZATION XIII – New Paradigm in Fluidization Engineering*, 2010, pp. 45-48.
- [11] Lavioletta J.-A., Patience G. S., Chaouki J. Fibre-Optic, Probe for Simultaneous Measurement of Gaseous Species Composition and Solids Volume Fraction, *Proceeding on International Conference FLUIDIZATION XIII – New Paradigm in Fluidization Engineering*, 2010, pp. 145-152.
- [12] Seville J. A., Single Particle View of Fluidization, *Proceeding on International Conference FLUIDIZATION XIII – New Paradigm in Fluidization Engineering*, 2010, pp. 9-16.
- [13] Deen N. G., Godiebed W., Gother S., Kuipers J. A. M., An Electrical Capacitance Tomography Study of Pressurized Fluidized Beds, *Proceeding on International Conference FLUIDIZATION XIII – New Paradigm in Fluidization Engineering*, 2010, pp. 161-168.
- [14] Mudde R. F., Fast X-Ray Tomography of a Bubbling Fluidized Bed, *Proceeding on International Conference FLUIDIZATION XIII – New Paradigm in Fluidization Engineering*, 2010, pp. 169-176.
- [15] Kohl M. H., Third J. R., Prussmann K. P., Muller C. R., A Magnetic Resonance Imaging (MRI) Study of the Formation and Interaction of Spouts and Jets, *Refereed Proceedings on the 14th International Conference on Fluidization – From Fundamentals to Products*, Engineering Conferences International ECI Digital Archives.
- [16] Muller C. R., Holland D. J., Sederman A. J., Gladden L. F., Dennis J. S., Magnetic Resonance (MR) Measurements of the Mass Flux in Gas-Solid Fluidized Bed, *Proceeding on International Conference FLUIDIZATION XIII – New Paradigm in Fluidization Engineering*, 2010, pp. 153-160.
- [17] Sancheza F. J., Briensa C., Berrutia F., Grayb M., McMillan J., Agglomerate Behaviour in a Recirculating Fluidized Bed with Sheds: Effect of Agglomerate Properties, *Refereed Proceedings on the 14th International Conference on Fluidization – From Fundamentals to Products*, Engineering Conferences International ECI Digital Archives.
- [18] J. Neuwirth, S. Antonyuk, S. Heinrich Analysis of the particle movement in dense granular flow, *Refereed Proceedings on the 14<sup>th</sup> International Conference on Fluidization – From Fundamentals to Products*, Engineering Conferences International ECI Digital Archives
- [19] Lykov A.V. *Theory of Heat Conduction*, Graduate School, 1967.
- [20] Cai Y., Cheng L., Xu L., Wang Q., Fang M., Luo Z., Nie L., Su H. NO<sub>x</sub> and N<sub>2</sub>O Emissions of Burning Coal with High Alkali Content in a Circulation Fluidized Bed // *Proceeding of the 22th International Conference on Fluidized Bed Conversion*, June 2015, Turku, Finland, pp. 496 – 503.
- [21] Yang H., Yang W., Yang Q., Wu S., Song Y., Ding X., Chen H. The Investigation of Gaseous Pollution and Co-Combustion Characteristics of

Tobacco Waste and Coal in a Chinese – Commercial Combined Heat and Power Plant // Proceeding of the 22th International Conference on Fluidized Bed Conversion, June 2015, Turku, Finland, pp. 192 – 197.

- [22] Borodulya V.A., Teplitsky Yu.S., Markevich I.I., Hassan A.F., Yeryomenko T.P., Heat and Mass Transfer Between a Surface and a Fluidized Bed Under Normal and Extreme Conditions, *Preprint № 2. Minsk. IFMO BSSR*, 1989.
- [23] Aerov M.E., Todes O.M., *Hydraulic and Thermal Fundamentals of the Operation of Apparatus with Fixed and Fluidized Bed of Granular Materials*, Khimiya. 1968.